Hindawi
Advances in Civil Engineering
Volume 2018, Article ID 5428670, 12 pages
https://doi.org/10.1155/2018/5428670

Research Article

An Experimental Study on Mechanical Behavior of Parallel Joint Specimens under Compression Shear

Fei Wang,[1] Ping Cao,[1] Yu Chen,[1,2] Qing-peng Gao,[1] and Zhu Wang[1]

[1]*School of Resource and Safety Engineering, Central South University, Changsha, Hunan, China*
[2]*State Key Laboratory for GeoMechanics and Deep Underground Engineering, Beijing 100083, China*

Correspondence should be addressed to Yu Chen; yu.chen@csu.edu.cn

Received 27 November 2017; Accepted 28 March 2018; Published 8 August 2018

Academic Editor: Dong-Sheng Jeng

In order to investigate the influence of the joint on the failure mode, peak shear strength, and shear stress-strain curve of rock mass, the compression shear test loading on the parallel jointed specimens was carried out, and the acoustic emission system was used to monitor the loading process. The joint spacing and joint overlap were varied to alter the relative positions of parallel joints in geometry. Under compression-shear loading, the failure mode of the joint specimen can be classified into four types: coplanar shear failure, shear failure along the joint plane, shear failure along the shear stress plane, and similar integrity shear failure. The joint dip angle has a decisive effect on the failure mode of the specimen. The joint overlap affects the crack development of the specimen but does not change the failure mode of the specimen. The joint spacing can change the failure mode of the specimen. The shear strength of the specimen firstly increases and then decreases with the increase of the dip angle and reaches the maximum at 45°. The shear strength decreases with the increase of the joint overlap and increases with the increase of the joint spacing. The shear stress-displacement curves of different joint inclination samples have differences which mainly reflect in the postrupture stage. From monitoring results of the AE system, the variation regular of the AE count corresponds to the failure mode, and the peak value of the AE count decreases with the increase of joint overlap and increases with the increase of joint spacing.

1. Introduction

The reliable assessment of rock masses is a common task in rock engineering. The discontinuities such as joints, faults, and bedding planes in the natural rock mass greatly weaken the stability of the rock mass [1–4]. These discontinuities control the mechanical properties of rock mass not only because of their interaction with the intact rock but also because of the interaction between themselves [5, 6]. When the specimen is loaded, new cracks develop near the tips of existing joints and propagate or coalesce with other cracks. The propagation of new cracks and the coalescence of fractures lead to a degradation in the mechanical properties of the rock. The effect law of joints on the failure of rock mass will have important guiding significance for actual engineering.

The mechanical behavior of nonpersistent jointed rock mass has been extensively studied by experiments and numerical simulation. Bobet and Einstein [7] identified five types of failure patterns from uniaxial compressive tests of gypsum specimens with parallel flaws. Wong and Chau [8] carried out uniaxial compression tests on plaster specimens with two flaws and identified nine types of coalescence patterns. Cao et al. [9] investigated the peak uniaxial compressive strength and failure patterns of ubiquitous-joint rock-like specimens by combining similar material testing and numerical simulation. The failure patterns of ubiquitous-joint specimens can be classified into four categories. Bahaaddini et al. [10] studied the effect of joint geometry parameters on the deformation modulus, compressive strength, and failure mode of the rock mass by particle flow modeling. Using photographic monitoring and acoustic emissions monitoring techniques, Yang et al. [11, 12] investigated the relationship between the real-time crack coalescence process and axial stress-time behavior for

red sandstone containing two unparallel fissures. Chen et al. [13] studied the influences of joint inclination angle and joint connectivity rate on compression strength and stress-strain curves of rock mass with nonpersistent open joints by conducting uniaxial compression tests on gypsum specimens. Fan et al. [14] performed numerical simulations to study the influence of multi-nonpersistent joints on mechanical behavior by using PFC3D software package. Yang et al. [15] numerically simulated the mechanical behavior of a jointed rock mass with nonpersistent joints adjacent to a free surface on the wall of an excavation.

The aforesaid experiments and numerical simulations illuminated the important influence of joint geometry on the mechanical behavior of rock masses under compression load. The interaction of rock bridges and the joint has been studied a lot [16, 17], whereas the interaction between joints has not been widely studied. Zhang et al. [3, 18] have studied the cracking and coalescence behavior in a rectangular rock-like specimen containing two parallel preexisting open flaws under uniaxial compression load. The results show that the spacing between two flaws and the inclination of a line linking up the inner flaw tips have different effects on the coalescence patterns and peak strength of specimens. Nevertheless, the interaction between joint planes in a nonpersistent jointed rock mass has rarely been investigated. And the jointed rock mass is often loaded by the comprehensive shear stress for the actual rock mass engineering, such as high and steep rock slope. The change of the rock mass with nonpersistent joints depends on joint configuration and loading conditions. Therefore, the research about the interaction between joints under comprehensive shear load will be significant. In this paper, the compression shear test loading on the parallel jointed specimens was carried out to look at the interaction of parallel joints and its effect on the failure mode, strength, and deformation behavior of jointed rock masses.

2. Experimental Program

2.1. Specimen Preparation. The specimens were made of white cement, water, and sand. The volume proportions ($V_{\text{water}} : V_{\text{white cement}} : V_{\text{silica sand}}$) in the specimens were 1 : 2 : 1. The dimensions (height × width × thickness) of each specimen were 100 mm × 100 mm × 30 mm. The existing joints were created by inserting mica sheets (0.6 mm thick; 15 mm long) into the fresh cement mortar paste at the desired location of the joints. The geometric parameters of the specimen and the distribution of joints are shown in Figure 1. Fissure geometry is defined by three geometrical parameters: joint dip angle, joint overlap, and joint spacing. The joint inclination of specimens have been defined as 0°, 30°, 45°, 60°, 75°, and 90°. For each dip angle, the joint overlap varied from 0 mm to 15 mm at 5-unit increments, and the joint spacing varied from 15 mm to 36 mm at 7-unit increments. The influence of joint orientation and joint overlap on the mechanical behavior of jointed rock mass was investigated by varying α and L_0, while keeping other geometric parameters constant (e.g., $d = 15$ mm, $L_r = 20$ mm, $L_j = 15$ mm). The influence of joint orientation and joint spacing on the mechanical behavior of jointed rock mass was investigated by varying α and d, while keeping other geometric parameters constant (e.g., $L_0 = 15$ mm, $L_r = 20$ mm, $L_j = 15$ mm).

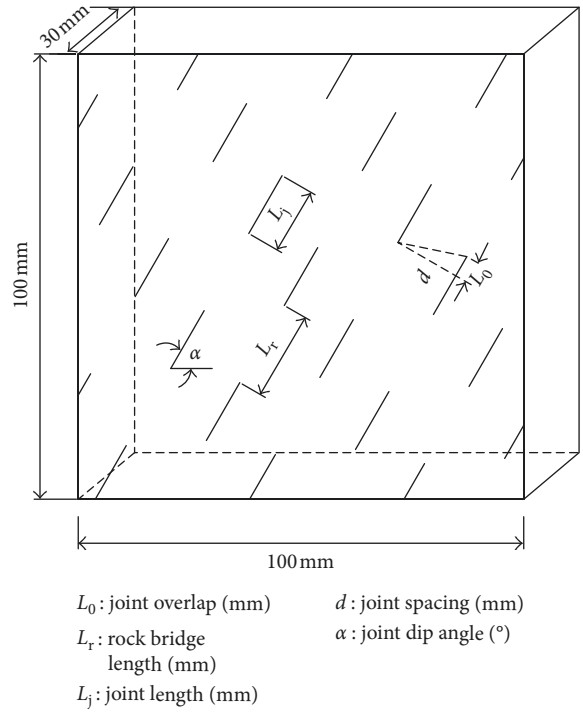

Figure 1: Geometrical parameters and joint arrangement.

Table 1: Mechanics parameters of rock-like material.

UCS (MPa)	Tensile strength (MPa)	Young's modulus (GPa)	Poisson's ratio	Cohesion (MPa)	Friction angle (°)
21.73	1.70	5.64	0.243	3.86	30.86

The specimens were not removed from the mold before the modeling material solidifies. Afterwards, the specimens were removed from the mold and soaked in water for 3 days and then were placed into a standard curing box (with the temperature kept at 20 ± 2 °C and humidity kept at 80%) for 25 days before mechanical testing. Three specimens were prepared for each joint distribution. Table 1 shows the fissure geometry information for all the specimens in this study. Each specimen was assigned an ID number using the notation S-*a*-*b*-*c*, where S stands for the sample, *a* represents joint overlap L_0, *b* is the joint spacing, and *c* is the inclination angle α. The mechanical properties of the intact sample, that is, the tensile strength, uniaxial compressive strength, internal friction angle, cohesion, elastic modulus, Poisson's ratio, are listed in Table 1.

2.2. Experimental Method. Figure 2 shows the shear box testing setup with the acoustic emission device attached to the specimen. The fixed compression shear angle is 45°. The compression shear tests were performed on the servocontrol

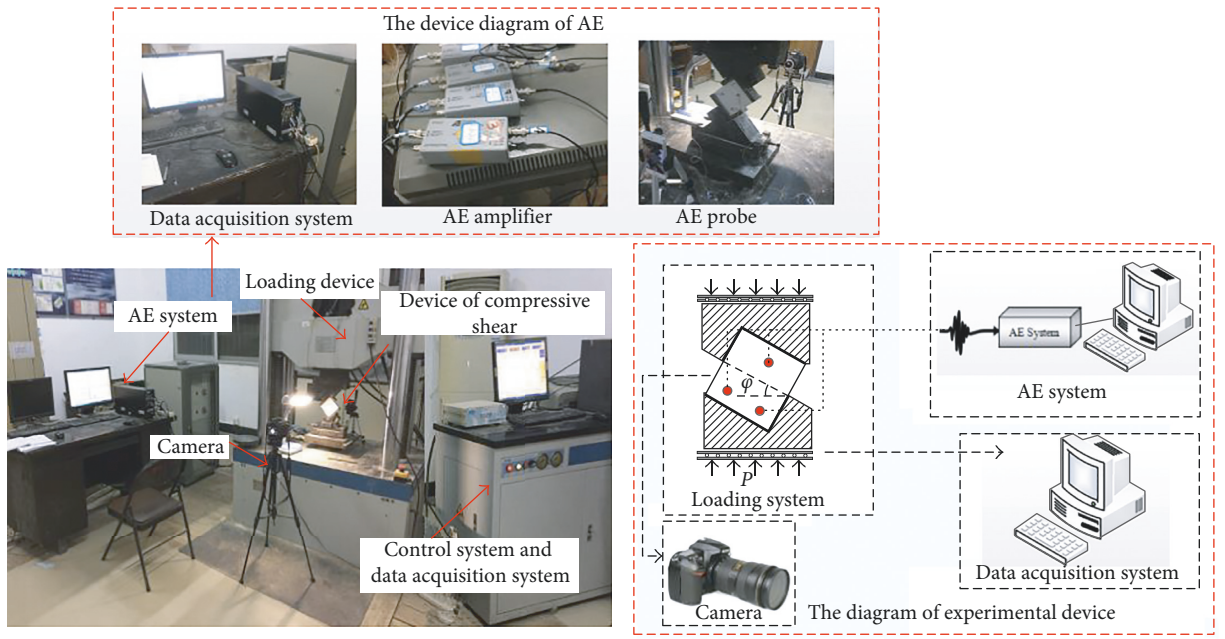

Figure 2: The device of the field test and schematic diagram.

loading instrument. The specimen was sandwiched between the two shear boxes. The loading was applied according to a displacement control manner. The loading was controlled by the loading control system (DCS-200). The loading rate was 0.1 mm/min. During the test, a digital camera was set up to take photographs of the specimen. The crack penetration and coalescence of the sample were monitored by acoustic emission. All specimens are loaded until specimen failure, and the load-displacement curves of the jointed samples are recorded simultaneously via a data acquisition system.

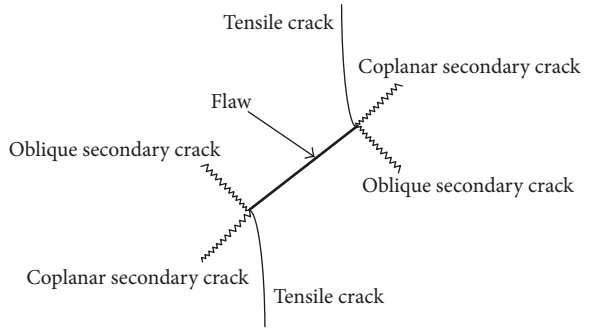

Figure 3: Crack types observed in preflawed specimens under load.

3. Effect of Parallel Joint on the Failure Mode of Samples

Prefabricated joints play a vital role in the failure of the specimen. Previous experimental and numerical results showed that when a load is applied to specimens with a single fissure, three types of cracks develop from the preexisting fissure (Figure 3): wing cracks, quasi-coplanar secondary cracks, and oblique secondary cracks. The axial load (Figure 4) can be decomposed into the shear load along the middle plane of the specimen and the compressive load along the upper plane of the specimen, and the shear load is equal to the compressive load at the compressive shear angle of 45°.

For ubiquitous-joint specimens, the mechanical behavior will be more complicated. When compression is applied to the existing flaws, tensile or shear cracks will develop from the tips of the existing fractures. As loading continues, these cracks will propagate and join with other cracks, by penetrating through the rock. Thus, the preexisting fissures will join with neighboring cracks, resulting in various types of failure patterns. According to the observation of the relationship between the failure surface and the

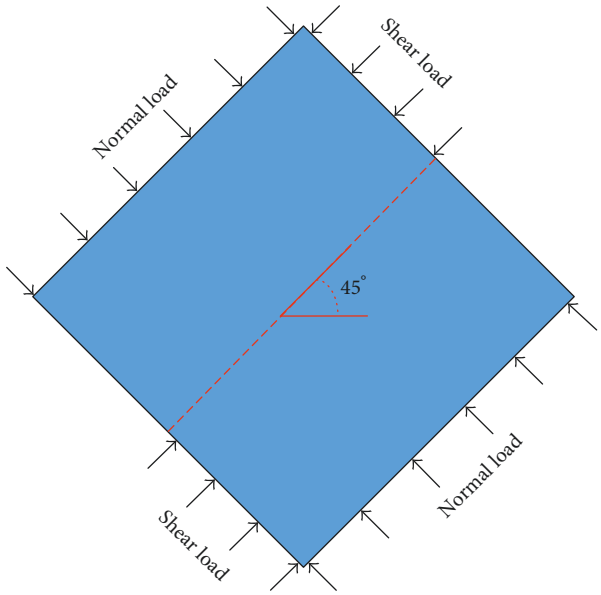

Figure 4: Diagram of stress analysis.

shear stress surface and the joint surface, the failure modes of ubiquitous-joint rock-like specimens can be generally classified into four categories: coplanar shear failure (failure mode I), shear failure along the joint plane (failure mode II), shear failure along the shear stress plane (failure mode III), and similar integrity shear failure (failure mode IV).

3.1. The Influence of Joint Inclination on Failure Modes of Samples. When the joint dip angle is 0°, wing cracks develop first from the joint tips under the compression shear load. The wing cracks are tensile cracks. And they initiate from the joint tips and propagate in a stable manner towards the direction of maximum compression (Figure 5(a)), which is consistent with the analytical results of the wing crack propagation in the classical fracture mechanics [19]. However, as the load increases, the shear stress starts to dominate the crack development. The propagation of wing crack does not continue and closes slowly. The shear stress plane of the specimen is coplanar with the joint surface. Therefore, the shear stress along the coplanar plane causes the crack to develop at both ends of the sample and overcome the bridge to expand. Ultimately, the cracks along the coplanar completely are cut through the specimen. The failure phenomenon is defined as a coplanar shear failure (failure mode I). As the shear load is equal to the axial load, the shear failure along the coplanar plane is more likely than compressive failure. Therefore, the failure path of the specimen is predictable, and the failure mode is a coplanar shear failure.

At $\alpha = 30^\circ$, the shear stress plane intersects the joint plane, and the failure mode of the specimen is complicated. Figure 5(b) shows that the specimen produces a large number of quasi-coplanar secondary cracks under compression shear stress. The quasi-coplanar secondary cracks develop from the tip of the joint at both ends of the shear stress plane and extend along the joint plane to break through the rock bridge. This failure is defined as shear failure along the joint plane (failure mode II). The failure mode of the 60° joint specimen is the same as that of the 30° joint specimen.

At $\alpha = 45^\circ$, the joint tip of the specimen produces oblique secondary cracks, quasi-coplanar secondary cracks, and wing cracks, as shown in Figure 5(c). Through the coalescence among the cracks, an irregular shear plane is formed in the middle of the sample. The failure of the specimen is similar to that of the integrity specimen. This failure is defined as similar integrity shear failure (failure mode IV).

When the joint dip angles are 75° and 90°, the shear stress plane is approximately perpendicular to the joint plane. Wing crack developed continuously in the middle of the specimen under compressive shear stress. As shown in Figures 5(e) and 5(f), with the increasing of the load, the shear stress dominates the crack development, and oblique secondary cracks develop from the tip of the joint near the shear plane and extend along the direction of the shear plane. Oblique secondary cracks constantly connect with the wing crack of the adjacent joints. Finally, a through-crack plane is formed parallel to the shear plane, which is defined as shear failure along the shear stress plane (failure mode III).

3.2. The Influence of Joint Overlap on Failure Modes of Samples. When the joint dip angle is 0°, the failure modes of the different joint overlap are failure mode I (Figure 5). With the decreasing joint overlap, more wing cracks are developed in the specimen under axial compression. However, with the increasing load, the shear stress along the shear plane dominates the failure of the specimen and promotes the closure of the wing crack. Finally, the specimens are destroyed by breaking through the rock bridge on the central shear plane. On the whole, the joint overlap only affects the number and distribution of wing cracks and does not change the failure mode of specimens. At $\alpha = 30^\circ$, the failure modes of the different joint overlap are failure mode II (Figure 5). As shown in Figure 5, the conclusion can be found that the change of the joint overlap did not change the failure mode under the same joint inclination, but only affected the number of crack growth and the expansion path. Because joint overlap only changes the relative position between joints without changing the joint density and the size of single joint is small, the joint overlap has almost no effect on failure modes.

3.3. The Influence of Joint Spacing on Failure Modes of Samples. In order to investigate the effect of joint spacing on the mechanical behavior of jointed rock mass, the joint spacing was varied to be 15 mm, 22 mm, 29 mm, and 36 mm. Correspondingly, the jointed rock mass have two, three, four, and four joint planes, respectively. The effect of joint spacing is studied in a range of the joint dip angle. The other geometric parameters are kept constant, that is, $L_0 = 15$ mm, $L_r = 20$ mm, and $L_j = 15$ mm. Table 2 displays the failure modes of jointed rock mass having a different joint spacing. It can be seen from Table 2 that, with the increase of the joint spacing, the joint dip plays an important role in the failure mode of the specimen. Under the same joint inclination, the joint specimens have similar failure modes at the different joint spacing, which shows that the joint inclination plays an important role in the failure mode.

When α is 0°, the failure modes of joint specimens with the different joint spacing are failure mode I. Although the increase of joint spacing changes the joint density of the specimen, it does not change the rock bridge length on the shear plane. Therefore, the failure modes of joint samples are the same. When α is 30, with the increases of joint spacing, the failure mode of the specimen changes from failure mode II to failure mode IV, which shows that the failure mode of the specimen changes gradually with the joint spacing increasing. It can be seen from Table 2 that the number of failure mode IV of joint specimens with joint spacing of 15 mm, 22 mm, 29 mm, and 36 mm, respectively, is 1, 2, 4, and 5. On the whole, with the increase of the joint spacing, the number of joints decreases, the weakest effect on the specimen decreases, and the number of specimens in

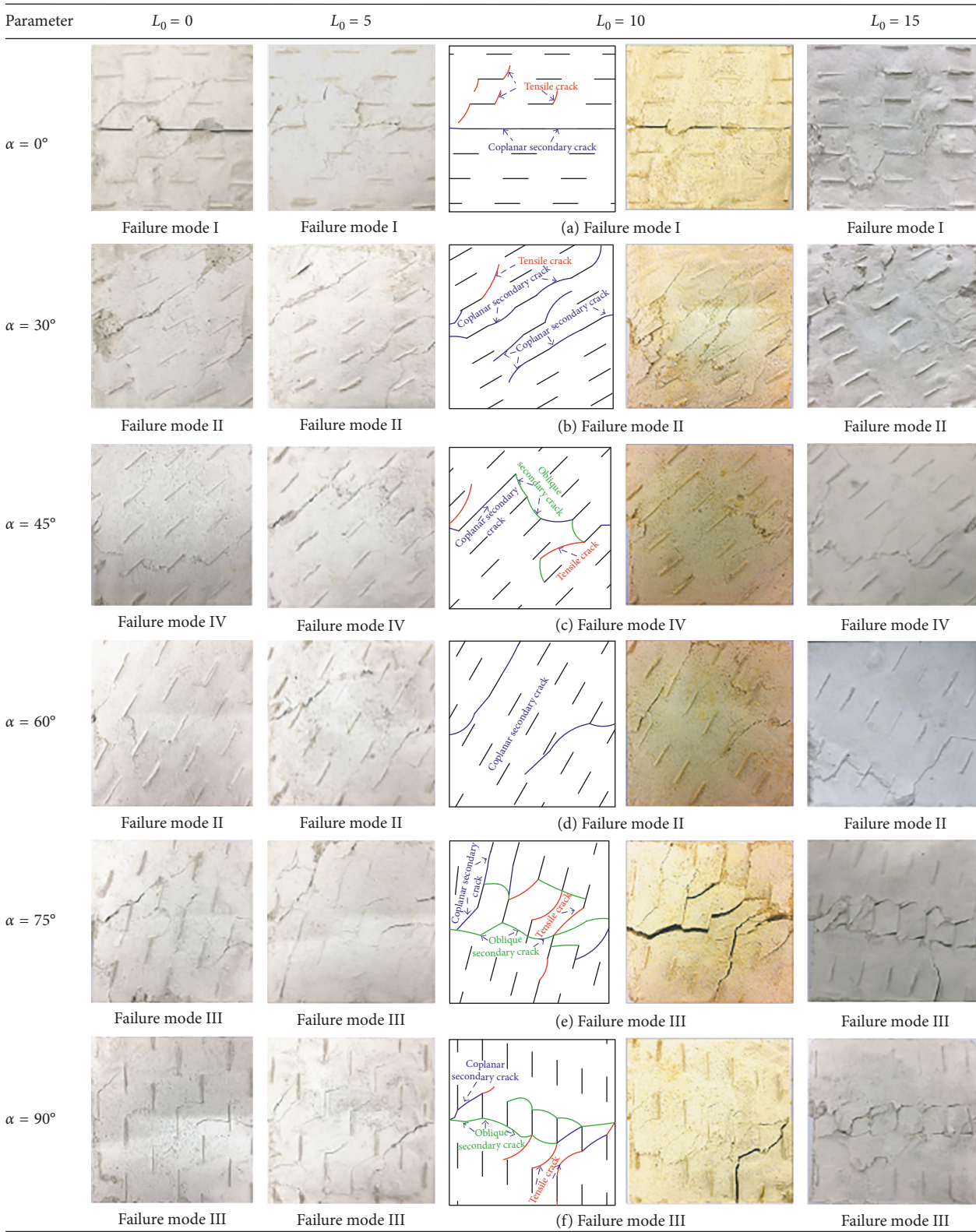

Figure 5: Failure modes of jointed rock mass.

failure mode IV increases. Therefore, the change of the joint spacing will cause the failure mode of the specimen to change, and the degree of influence is related to the joint inclination.

4. Influence of Parallel Joint on Sample Strength

In this experiment, the compression shear angle is 45°, and the compression stress loading on the specimen is equal to

Table 2: Failure modes for specimens with the different joint inclination and joint spacing.

Joint inclination α	Joint spacing d (mm)			
	15	22	29	36
0°	Failure mode I	Failure mode I	Failure mode I	Failure mode I
30°	Failure mode II	Failure mode II	Failure mode IV	Failure mode IV
45°	Failure mode IV	Failure mode IV	Failure mode IV	Failure mode IV
60°	Failure mode II	Failure mode IV	Failure mode IV	Failure mode IV
75°	Failure mode III	Failure mode III	Failure mode IV	Failure mode IV
90°	Failure mode III	Failure mode III	Failure mode III	Failure mode IV

the shear stress. The compression shear tests of joint samples were conducted. The peak shear strength of the joint specimens is shown in Table 3.

4.1. The Effect of Joint Inclination on the Shear Strength of the Specimens. The joint inclination has a great influence on the peak shear strength which presents a certain law (Figure 6). When the dip angle increases from 0° to 45°, the peak shear strength of the specimens shows an increasing trend. From 45° to 90°, the peak shear strengths begin to decrease with the increase of the dip angle. All of the specimens for the different joint overlap reach the maximum value of the peak shear strength at 45°. The joint specimen gets the maximum shear strength at $\alpha = 45°$ and $L_0 = 0$ mm which is 9.42 MPa. The peak shear strength is affected by the failure modes of the specimens.

When the joint dip angle $\alpha = 0°$, the failure modes of the joint specimens are failure mode I. In the failure mode, joint length on the failure plane is comparatively long and the rock bridge is relatively short. At the same time, the shear stress is concentrated along the joint plane. This is the reason why it is easy to develop quasi-coplanar secondary cracks to break the sample, and the shear strength is relatively small. While the joint dip angle $\alpha = 30°$ or 60°, the failure modes of the joint specimens are failure mode II. The cracks are dominated by the secondary crack in the plane. Owing to the shear stress that cannot be concentrated to the failure surface, the shear strength will increase. At $\alpha = 45°$, the failure modes of the joint specimens are failure mode IV. The joint weakening effect is the smallest, and thus, the peak shear strength is the largest. When the joint dip angles are 75° and 90°, the failure modes of the joint specimen are dominated by failure mode III. The shear stress plane is approximately perpendicular to the joint plane. The joints are concentrated in the middle of the specimen. The shear stress-dominated oblique secondary cracks continue to develop and expand, through the sample. The peak shear strength is smaller than 60°, and the 90° joint specimen is more susceptible to damage than 75°.

4.2. The Effect of Joint Overlap on the Shear Strength of the Specimens. Figure 5 shows the effect of joint overlap on the peak shear strength. It can be seen from Figure 7 that the overlap length has a major influence on the peak shear strength of the specimens. In Figure 7, the peak shear strength decreases with the increase of the overlap length; the maximum value is observed at $L_0 = 0$ mm, and the minimum value is observed at $L_0 = 15$ mm. At the same joint inclination angle, with the change of the joint overlap, the failure modes are the same and the joint density of the samples is roughly equal, but the uniformity of the joint distribution changes. The smaller the degree of the joint overlap is, the more uniform the distribution of joints on the specimen is. Under the compressive shear stress, the joints of the specimen are more concentrated, and the damage is easier to occur. Thus, the peak shear strength decreases with the increase of the overlap length. In the experimental results, as the overlapping length increases from 0 mm to 15 mm, the peak shear strength of $\alpha = 0°$, 30°, and 45°samples decrease by approximately 47.1%, 39.0%, and 21.2%, respectively.

4.3. The Effect of Joint Spacing on the Shear Strength of the Specimens. The effect of the joint spacing on peak shear strength is shown in Figure 8. At the same joint inclination angle, the peak shear strength of specimens increases with the increase of joint spacing. The maximum peak shear strength is obtained for a specimen with $d = 36$ mm, and the minimum peak shear strength is for $d = 15$ mm. The increase of the joint spacing leads to the increase of the rock bridge length between prefabricated joints, so the joint specimen is more difficult to break. Therefore, the larger the joint spacing is, the greater the peak shear strength is. At $\alpha = 75°$, the peak shear strength of specimens with the joint spacing of 15 mm, 22 mm, 29 mm, and 36 mm is 5.18, 6.51, 7.12, and 7.17 MPa, respectively, and the relative growth rate of peak shear strength is 25.7%, 9.4%, and 0.7%. The increase of the joint spacing in the real rock mass leads to the decrease of the joint density. However, due to the constant sample size in this experiment, some joint spacing changes did not result in an increase in joint density. In this test, the width of specimens is 100 mm, and the parallel joint specimens of spacing of 29 mm and 36 mm both have 3 rows joints. Therefore, the peak shear strength of specimens with 29 mm and 36 mm joint spacing in the same joint inclination is similar.

The peak shear strength of the joint specimen is related to its corresponding failure mode. It can be seen from the failure modes of the joint specimens in Table 2 that, with the increase of joint spacing, the number for failure mode IV of specimens increase. At $\alpha = 60°$, the joint spacing increases from 15 mm to 22 mm, and the failure mode transforms from failure mode II to failure mode IV. At $\alpha = 75°$, the specimen joint spacing increases from 22 mm to 29 mm, and the failure mode changes from failure mode III to failure mode IV. At $\alpha = 90°$, the specimen joint spacing increases

Table 3: The shear strength of joint specimens.

Number	Sample ID	Shear strength (MPa)	Number	Sample ID	Shear strength (MPa)	Number	Sample ID	Shear strength (MPa)
1	S-0-15-0	7.86	15	S-10-15-45	7.64	29	S-15-22-75	6.51
2	S-0-15-30	9.11	16	S-10-15-60	6.7	30	S-15-22-90	5.25
3	S-0-15-45	9.42	17	S-10-15-75	6.02	31	S-15-29-0	5.07
4	S-0-15-60	8.83	18	S-10-15-90	5.45	32	S-15-29-30	7.39
5	S-0-15-75	7.56	19	S-15-15-0	4.16	33	S-15-29-45	7.91
6	S-0-15-90	7	20	S-15-15-30	5.56	34	S-15-29-60	7.66
7	S-5-15-0	6.18	21	S-15-15-45	7.42	35	S-15-29-75	7.12
8	S-5-15-30	8.14	22	S-15-15-60	6.41	36	S-15-29-90	5.67
9	S-5-15-45	8.36	23	S-15-15-75	5.18	37	S-15-36-0	4.95
10	S-5-15-60	7.26	24	S-15-15-90	4.33	38	S-15-36-30	7.38
11	S-5-15-75	6.29	25	S-15-22-0	4.58	39	S-15-36-45	8.06
12	S-5-15-90	5.55	26	S-15-22-30	7.25	40	S-15-36-60	7.82
13	S-10-15-0	5.05	27	S-15-22-45	7.54	41	S-15-36-75	7.17
14	S-10-15-30	6.17	28	S-15-22-60	7.32	42	S-15-36-90	5.81

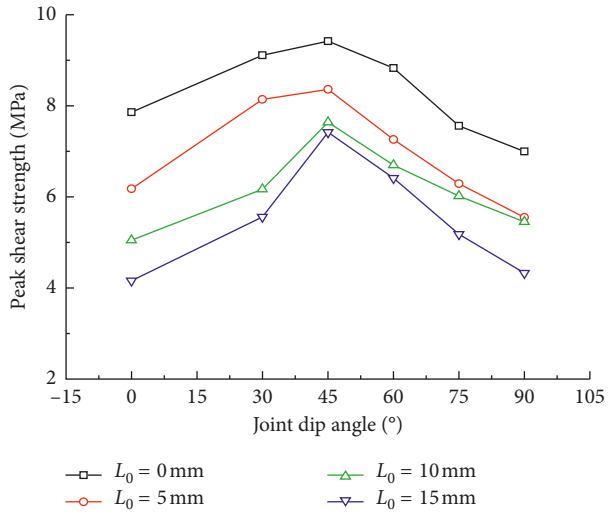

Figure 6: Effect of the inclination angle of the joint on the peak shear strength.

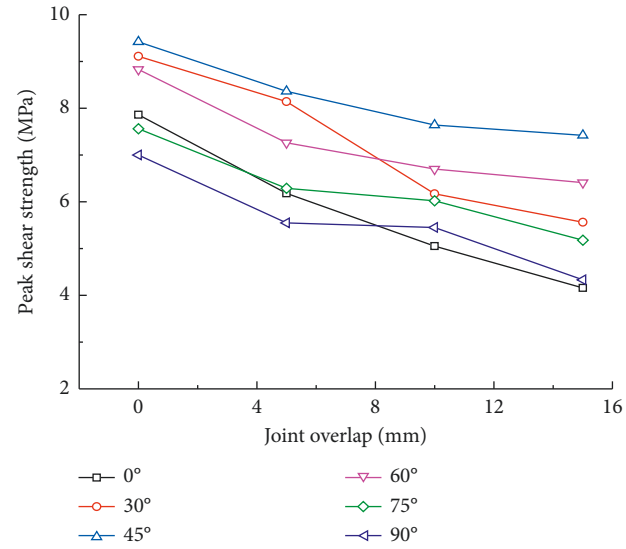

Figure 7: Effect of the joint overlap on the peak shear strength.

from 29 mm to 36 mm, and the failure mode transforms from failure mode III to failure mode IV. At the same joint inclination, the peak shear strength of specimens with failure mode IV is larger than the other samples with the other failure modes, so the peak shear strength of joint specimens increases with the increase of the joint spacing.

5. Shear Stress-Displacement Curve and AE Analysis

Based on the study of the failure mode and strength of the joint specimen, the shear stress-displacement curve combined with the acoustic emission is used to quantitatively investigate the crack initiation, expansion, and penetration of the specimen. The regular crack development is studied in detail which will help to observe the influence of joint geometry on the curve and the correlation between shear stress-displacement curve and failure mode and strength. The study will deepen the understanding of the mechanical behavior of joints under compressive shear stress.

From the start to the failure during testing, the shear stress-displacement curve of samples combined with acoustic emission counts (Figure 9) can be divided into four typical stages: the microfracture closure stage (OA), the elastic stage (AB), the rupture stage (BC), and the postrupture stage (CD). At the microfracture closure stage, the sample is gradually compost under the load due to the closed joints and voids, and the early nonlinear curves are formed. The acoustic emission activity is active, the counting value is greater, and the range of change is larger. During the elastic stage, the shear stress and displacement of the rock bridge are linearly related to each other. The interior of the rock bridge is filled with a large number of elastic properties under loading. The slope of the elastic stage is obviously higher than that of the microfracture closure stages. As the crack development reduces, the acoustic emission reduces and becomes stable. In the rupture stage, the curve slope gradually decreases, and the

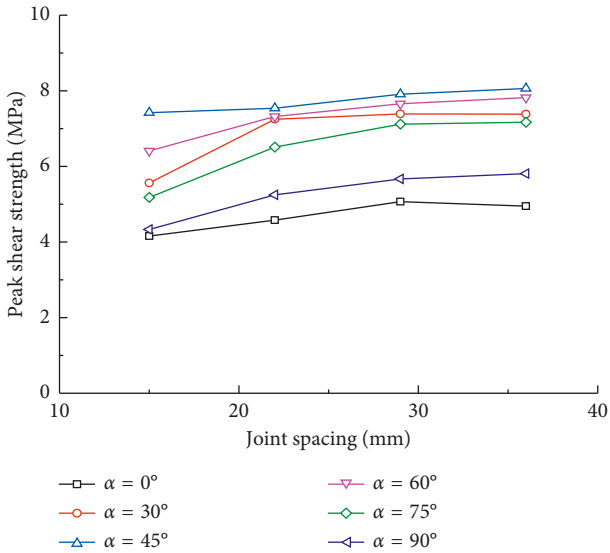

Figure 8: Effect of the joint spacing on the peak shear strength.

curve reaches the peak shear strength. The cracks of the sample joint tip continue to expand and coalescence through overcoming the rock bridge resistance. The active degree of acoustic emission gradually increases. The count of acoustic emission starts to increase from the point B and shows a geometric increase afterwards until the maximum count appears at this stage. In the postrupture stage, as the displacement increases, the shear stress decreases continuously. The rock bridge is broken to form the destructive plane which leads to the sudden drop of stress caused by the local frictional slippage. Finally, the count of acoustic emission begins to decrease.

5.1. Influence of Joint Inclination on Shear Stress-Displacement Curve and AE Analysis. The shear stress-displacement curves (Figure 9(a)) have some differences especially in the postrupture stage with the changes of joint inclination. Taking the overlap of 15 mm as an example, in the postrupture stage, the sudden drop of stress occurs only at the sample of 45° joint, and the stress at the other inclinations decrease slowly. The descending rate of the curve with different samples of joint inclination is different, and the descending rate of the stress is related to the failure mode of the specimen. The failure mode of the 45° specimen is similar integrity shear failure. Due to the sudden release of a large amount of energy inside the sample, the stress-displacement curve produces the phenomenon of sudden descent of stress. The failure modes of 30° and 60° specimens are shear failures along the joint plane. Due to the release of aggregated energy, the descending rate of the curve in the postrupture stage is relatively slower than that of 45°. The failure modes of 75° and 90° specimens are shear failures along the shear stress plane. The peak shear strength of the specimen is small. During the loading process, the cracks develop evenly and the energy accumulation is less. Therefore, the descending rate of the curve in the postrupture stage is relatively small. The failure modes of the 0° specimen are the coplanar shear failure. The stress-displacement curve is relatively gentle, and the descending rate is the smallest. On the whole, the descending rates of the curve are positively correlated with the peak strength of the sample. The stress-displacement curves of the specimen with the overlap of 0 mm appear single or multilevel stresses abruptly in the postrupture phase. The curves of specimens at the joint dip angle of 45°, 30°, 60°, and 0° occur the phenomenon of single-stage stress drop, and the curves of samples at the 75°, 90° appear multilevel stresses abruptly. The relationship between the descending rate of the curve and the joint inclination of the sample is similar to that of the sample of 15 mm overlap. Compared with the specimens in the different overlap, the curves of samples with 0 mm overlap are prone to sudden stress drop, and the descending rate is greater. On the whole, the descending rates of the curve are positively correlated with the peak strength of the sample.

According to the change of acoustic emission count (Figure 9(b)), the acoustic emission activities can be divided into the active period, the clam period, and the acute period. The acoustic emissions of samples with different inclinations have certain differences. When the joint dip angle is 0°, the acoustic emission is relatively active in the stage of microcrack closure and enters the clam period in the elastic stage and then the acute period with geometric growth in the rupture and postrupture stage. Compared with the acoustic emission of the 0° joint sample, the acoustic emission count of the 30° joint sample changes greatly in the active period and decreased rapidly due to the sudden stress drop in the postrupture. The clam period of the 45° specimen is relatively short. The AE count progressively increases in the acute period which is related to the more development of the crack before the failure of the specimen. For the 75° joint specimen, due to the multilevel stress drop in the stress-displacement curve, the acoustic emission counts also show multiple peaks. On the whole, the variation law of acoustic emission is consistent with the joint dip angle, and the joint angle of the specimen plays a key role in the failure mode. Therefore, the failure mode is corresponding to the variation of the acoustic emission count.

5.2. Influence of Overlap Length on Shear Stress-Displacement Curve and AE Analysis. As shown in Figure 10(a), the smaller the overlap length is, the larger the peak shear strength and displacement are. Even the curve shapes of the sample for different overlap lengths are similar, and the curve slopes change especially in the postrupture stage. For example, the curves of the different overlap are gentle when $\alpha = 0°$. The curves decrease gradually in the postrupture stage. The smaller the overlap is, the faster the descent rate is. At $\alpha = 45°$, the specimens have a significant stress drop in the postrupture stage. At the same time, with the decrease of overlap, the value of stress drop increases.

As shown in Figure 10(b), at $\alpha = 0°$, the variation rules of acoustic emission counts with the different overlap are similar, and the peak value of the AE count decreases with the increase of the joint overlap. The similar variation is due to the same failure mode of the specimens. The peak value of the AE count is related to the shear strength of samples. The

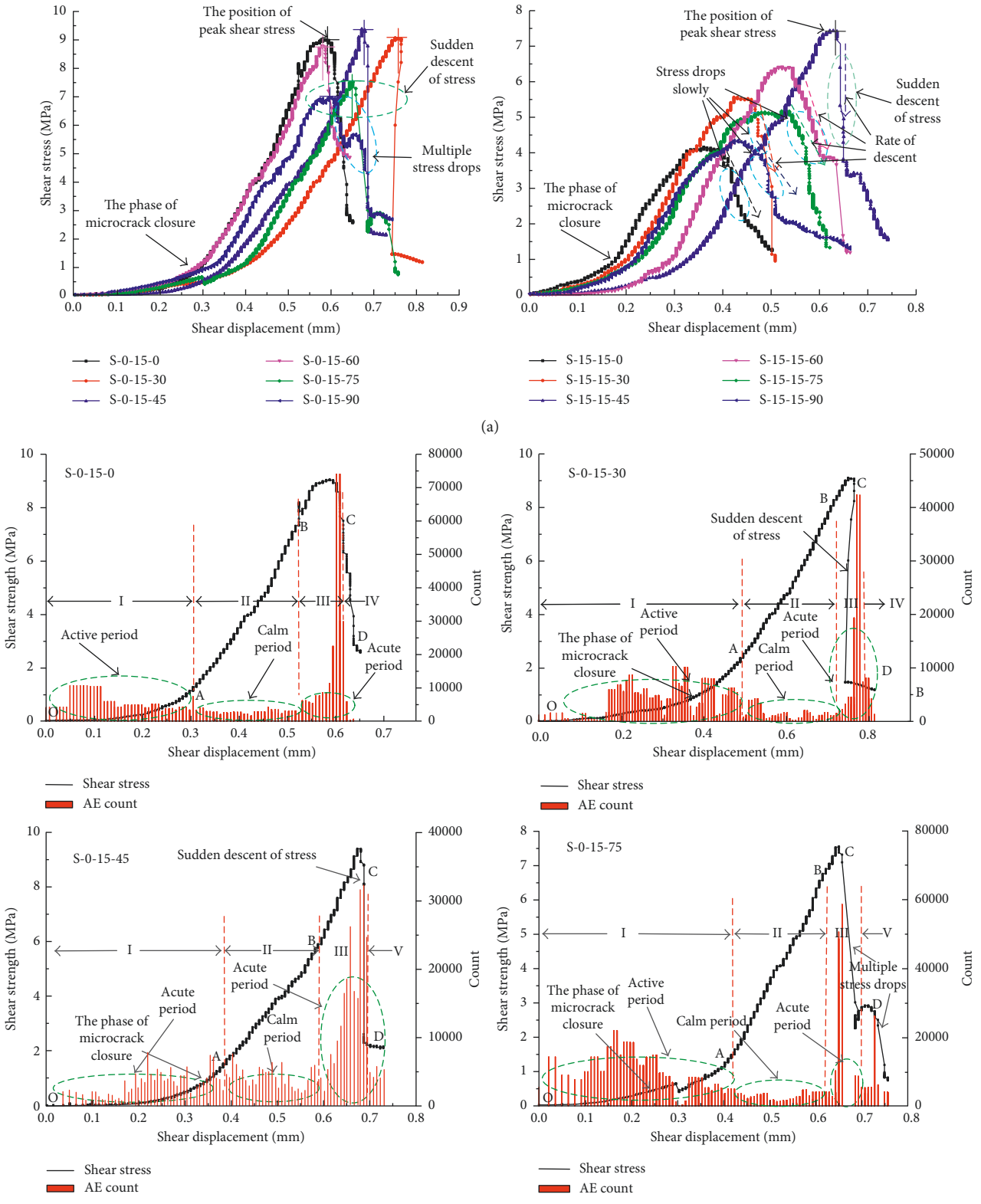

FIGURE 9: The effect of joint inclination on the shear stress-displacement curve and AE count: (a) the shear stress-shear displacement curves of different joint inclinations; (b) the variation of acoustic emission count for different angle specimens.

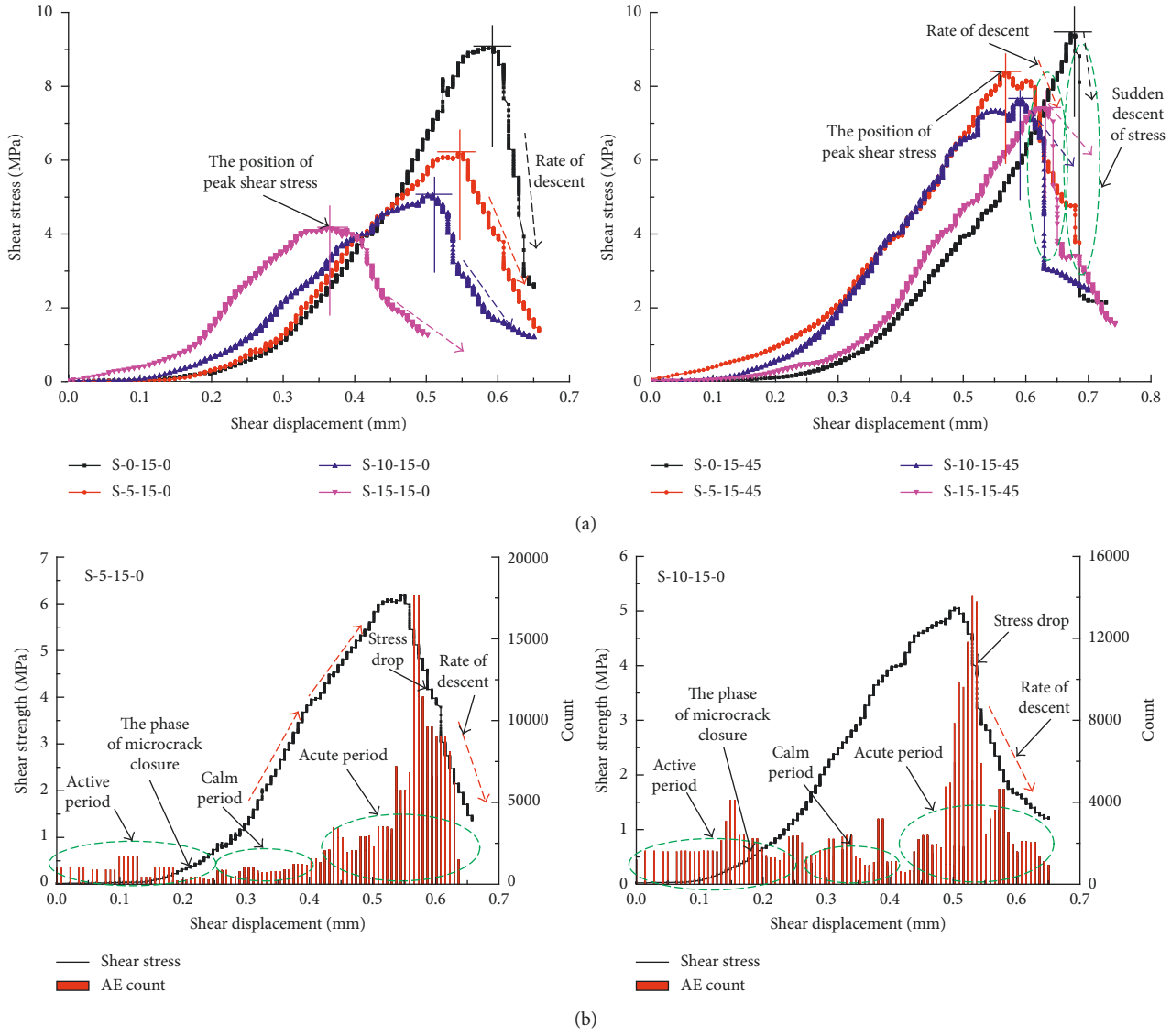

FIGURE 10: The effect of joint overlap on the shear stress-displacement curve and AE count: (a) the shear stress-displacement curve of samples containing different joint overlap lengths; (b) the variation of acoustic emission counts for different overlapping specimens.

shear strength of the specimen increases with the decrease of the joint overlap. The larger the peak shear strength is, the greater the energy of the emission is. Thus, the peak value of the AE count is greater.

5.3. Influence of Joint Spacing on Shear Stress-Displacement Curve and AE Analysis. The shear stress-displacement curve (Figure 11(a)) shows that the larger the joint spacing is, the larger the peak shear strength is. The curves of samples with the different joint spacing are similar. However, the slope of the curve varies with the change of the joint spacing. For the specimens with 0°joint inclination, the curves of the samples with the different joint spacing change gently and decrease gradually. The larger the spacing of joints, the faster the rate of descent is. For the specimens with 60° joint inclination, the curves have a suddenly descent of stress in the postrupture stage, and the larger the joint spacing, the greater the value of the sudden drop in stress.

As shown in Figure 11(b), the variation rules of acoustic emission counts correspond to the shear stress-displacement curve of samples. For example, the curve of the S-15-22-45 sample produces two sudden drops of stress, and the varied form of the acoustic emission count also has two peaks. The variation rules of acoustic emission counts with the different spacing are similar, and the peak value of the AE count increases with the increase of the joint spacing. The similar variation is due to the same failure mode of the specimens. The peak value of the AE count is related to the shear strength of samples. The shear strength of the specimen increases with the increase of the joint spacing. The larger the peak shear strength is, the greater the energy of the emission is. Thus, the peak value of the AE count is greater.

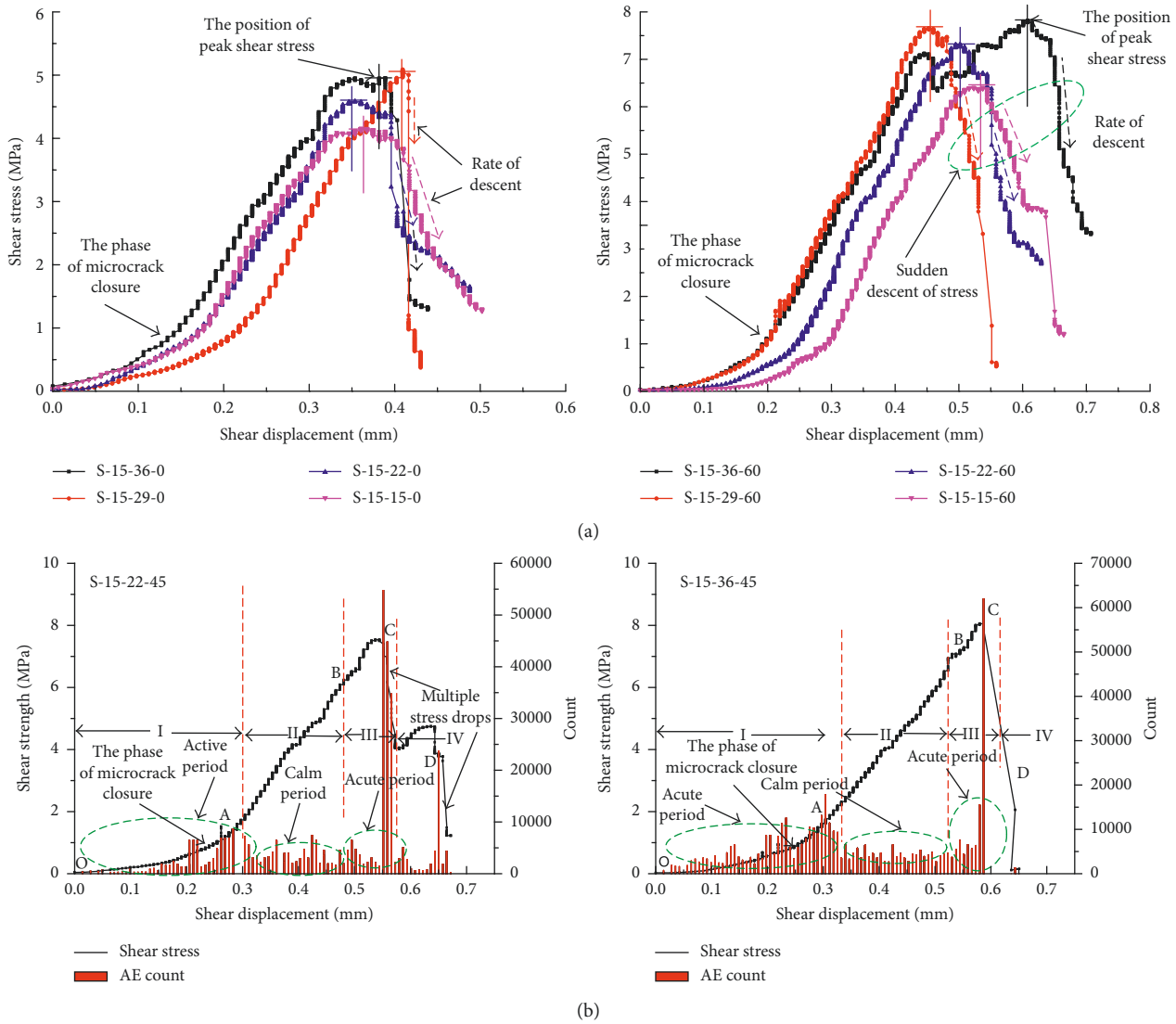

FIGURE 11: The effect of joint spacing on the shear stress-displacement curve and AE count: (a) the shear stress-shear displacement curves with the different joint spacing; (b) the variation of acoustic emission count for different spacing specimens.

6. Conclusions

A series of jointed rock mass specimens prepared with rock-like materials were utilized to investigate the effect of the parallel joint on the mechanical behavior of rock mass under compression shear. From the experimental results, the following conclusions can be drawn:

(1) According to the relationship between the failure surface and the shear stress plane and the joint surface, four basic failure modes of the specimen are coplanar shear failure, shear failure along the joint plane, shear failure along the shear stress plane, and similar integrity shear failure. The joint dip angle plays a decisive role in the failure mode of the specimen. The joint overlap affects the crack development of the specimen but does not change the failure mode of the specimen. The joint spacing can change the failure mode of the specimen, and the degree of influence is related to the joint inclination.

(2) The peak shear strength increases firstly and then decreases with the increase of joint dip angle and reaches the maximum value at 45°. With the increase of joint overlap, the peak shear strength decreases. The peak shear strength of specimens increases with the increase of joint spacing.

(3) The shear stress-displacement curve of samples combined with acoustic emission counts can be divided into four typical stages: the microfracture closure stage, the elastic stage, the rupture stage, and the postrupture stage. The shear stress-displacement curve of different joint inclination samples is different, and it mainly occurs in the postrupture stage. The shear stress-displacement curves of specimens in the same failure modes are similar.

(4) The variation of the AE count for different inclination joint specimens is consistent with the failure mode of the specimen. The variation rules of acoustic emission counts with the different overlap are similar, and with the joint overlap increasing, the peak value of the AE count decreases. The peak value of the AE count increases with the increase of the joint spacing.

Conflicts of Interest

The authors declare that they have no conflicts of interest.

Acknowledgments

The authors would like to acknowledge these financial supports: Project (2017zzts164) supported by the Fundamental Research Funds for the Central Universities, China; Projects (11772358 and 51604299) supported by the National Natural Science Foundation of China; the State Key Research Development Program of China (2016YFC0600706); the China Postdoctoral Science Foundation (2016M600636); Project (SKLGDUEK1724) funded by the Open Projects of State Key Laboratory for Geomechanics and Deep Underground Engineering, Beijing; and the China Postdoctoral International Exchange Introduction Project.

References

[1] C. A. Tang, P. Lin, R. H. C. Wong, and K. T. Chau, "Analysis of crack coalescence in rock-like materials containing three flaws–part II: numerical approach," *International Journal of Rock Mechanics and Mining Sciences*, vol. 38, no. 7, pp. 925–939, 2001.

[2] X. Fan, K. Li, H. Lai, Y. Xie, R. Cao, and J. Zheng, "Internal stress distribution and cracking around flaws and openings of rock block under uniaxial compression: a particle mechanics approach," *Computers and Geotechnics*, vol. 102, no. 10, pp. 28–38, 2018.

[3] X. P. Zhang and L. N. Y. Wong, "Crack initiation, propagation and coalescence in rock-like material containing two flaws: a numerical study based on bonded-particle model approach," *Rock Mechanics and Rock Engineering*, vol. 46, no. 5, pp. 1001–1021, 2013.

[4] X. X. Yang, H. W. Jing, C. A. Tang, and S.-Q. Yang, "Effect of parallel joint interaction on mechanical behavior of jointed rock mass models," *International Journal of Rock Mechanics and Mining Sciences*, vol. 92, pp. 40–53, 2017.

[5] P. Cao, T. Y. Liu, C. Z. Pu, and H. Lin, "Crack propagation and coalescence of brittle rock-like specimens with pre-existing cracks in compression," *Engineering Geology*, vol. 187, no. 17, pp. 113–121, 2015.

[6] M. Wang, P. Cao, W. Wan, Y.-L. Zhao, J. Liu, and J.-S. Liu, "Crack growth analysis for rock-like materials with ordered multiple pre-cracks under biaxial compression," *Journal of Central South University*, vol. 24, no. 4, pp. 866–874, 2017.

[7] A. Bobet and H. H. Einstein, "Fracture coalescence in rock-type materials under uniaxial and biaxial compression," *International Journal of Rock Mechanics and Mining Sciences*, vol. 35, no. 7, pp. 863–888, 1998.

[8] R. H. C. Wong and K. T. Chau, "Crack coalescence in a rock-like material containing two cracks," *International Journal of Rock Mechanics and Mining Sciences*, vol. 35, no. 2, pp. 147–164, 1998.

[9] R. H. Cao, P. Cao, X. Fan, X. Xiong, and H. Lin, "An experimental and numerical study on mechanical behavior of ubiquitous-joint brittle rock-like specimens under uniaxial compression," *Rock Mechanics and Rock Engineering*, vol. 49, no. 11, pp. 4319–4338, 2016.

[10] M. Bahaaddini, G. Sharrock, and B. K. Hebblewhite, "Numerical investigation of the effect of joint geometrical parameters on the mechanical properties of a non-persistent jointed rock mass under uniaxial compression," *Computer Geotechnical*, vol. 49, pp. 206–225, 2013.

[11] S. Q. Yang, W. L. Tian, Y. H. Huang, P. G. Ranjith, and Y. Ju, "An experimental and numerical study on cracking behavior of brittle sandstone containing two non-coplanar fissures under uniaxial compression," *Rock Mechanics and Rock Engineering*, vol. 49, no. 4, pp. 1497–1515, 2016.

[12] S. Q. Yang, X. R. Liu, and H. W. Jing, "Experimental investigation on fracture coalescence behavior of red sandstone containing two unparallel fissures under uniaxial compression," *International Journal of Rock Mechanics and Mining Sciences*, vol. 63, no. 5, pp. 82–92, 2013.

[13] X. Chen, Z. H. Liao, and D. J. Li, "Experimental study of effects of joint inclination angle and connectivity rate on strength and deformation properties of rock masses under uniaxial compression," *Chinese Journal of Rock Mechanics and Engineering*, vol. 30, no. 4, pp. 781–789, 2011.

[14] X. Fan, P. H. S. W. Kulatilake, and X. Chen, "Mechanical behavior of rock-like jointed blocks with multi-non-persistent joints under uniaxial loading: a particle mechanics approach," *Engineering Geology*, vol. 190, pp. 17–32, 2015.

[15] X. X. Yang, P. H. S. W. Kulatilake, H. W. Jing, and S. Yang, "Numerical simulation of a jointed rock block mechanical behavior adjacent to an underground excavation and comparison with physical model test results," *Tunnelling and Underground Space Technology*, vol. 50, pp. 129–142, 2015.

[16] H. Lee and S. Jeon, "An experimental and numerical study of fracture coalescence in pre-cracked specimens under uniaxial compression," *International Journal of Solids and Structures*, vol. 48, no. 6, pp. 979–999, 2011.

[17] C. H. Park and A. Bobet, "Crack initiation, propagation and coalescence from frictional flaws in uniaxial compression," *Engineering Fracture Mechanics*, vol. 77, no. 14, pp. 2727–2748, 2010.

[18] X. P. Zhang, Q. S. Liu, S. C. Wu, and X. H. Tang, "Crack coalescence between two non-parallel flaws in rock-like material under uniaxial compression," *Engineering Geology*, vol. 199, pp. 74–90, 2015.

[19] Q. H. Rao, Z. Q. Sun, O. Stephansson, C. Li, and B. Stillborg, "Shear fracture (mode II) of brittle rock," *International Journal of Rock Mechanics and Mining Sciences*, vol. 40, no. 3, pp. 355–375, 2003.